Published in final edited form as:
Nature. 2016 September 15; 537(7620): 394–398. doi:10.1038/nature18956.

A nucleosynthetic origin for the Earth's anomalous ^{142}Nd composition

C. Burkhardt[1,2], **L.E. Borg**[3], **G.A. Brennecka**[2,3], **Q.R. Shollenberger**[2,3], **N. Dauphas**[1], and **T. Kleine**[2]

[1]Origins Laboratory, Department of the Geophysical Sciences and Enrico Fermi Institute, The University of Chicago, 5734 South Ellis Avenue, Chicago, IL 60637, USA

[2]Institut für Planetologie, Westfälische Wilhelms-Universität Münster, Wilhelm Klemm-Strasse 10, 48149 Münster, Germany

[3]Lawrence Livermore National Laboratory, L231, Livermore, CA 94550, USA

Abstract

A long-standing paradigm assumes that the chemical and isotopic composition of many elements in the bulk silicate Earth are the same as in chondrites1–4. However, the accessible Earth has a greater ^{142}Nd/^{144}Nd than chondrites. Because ^{142}Nd is the decay product of now-extinct ^{146}Sm ($t_{1/2}$= 103 million years5), this ^{142}Nd difference seems to require a higher-than-chondritic Sm/Nd of the accessible Earth. This must have been acquired during global silicate differentiation within the first 30 million years of Solar System formation6 and implies the formation of a complementary ^{142}Nd-depleted reservoir that either is hidden in the deep Earth6, or was lost to space by impact erosion3,7. Whether this complementary reservoir existed, and whether or not it has been lost from Earth is a matter of debate3,8,9, but has tremendous implications for determining the bulk composition of Earth, its heat content and structure, and for constraining the modes and timescales of its geodynamical evolution3,7,9,10. Here, we show that compared to chondrites, Earth's precursor bodies were enriched in Nd produced by the slow neutron capture process (*s*-process) of nucleosynthesis. This *s*-process excess leads to higher ^{142}Nd/^{144}Nd, and, after correction for this effect, the ^{142}Nd/^{144}Nd of chondrites and the accessible Earth are indistinguishable within 5 parts per million. The ^{142}Nd offset between the accessible silicate Earth and chondrites, therefore, reflects a higher proportion of *s*-process Nd in the Earth, and not early differentiation processes. As such, our results obviate the need for hidden reservoir or super-chondritic Earth models, and imply a chondritic Sm/Nd for bulk Earth. Thus, although chondrites formed at greater heliocentric distance and contain a different mix of presolar components than Earth, they nevertheless are suitable proxies for Earth's bulk chemical composition.

Correspondence or requests for materials can be addressed to C.B. (burkhardt@uni-muenster.de).

Author contributions: CB initiated the project in collaboration with LB, ND and TK, acquired and processed the samples in Chicago and wrote a first draft of the manuscript. LB, GB and QS performed additional chemistry and measured all samples in Livermore. All authors contributed to the data interpretation and editing of the manuscript.

The authors declare no competing financial interests.

Author information: Data are also available via the EarthChem library DOI:XXX.

Europe PMC Funders Author Manuscripts

Coupled ^{146,147}Sm-^{142,143}Nd systematics are a powerful tool to constrain the timescales and processes involved in the early differentiation of Earth, the Moon and Mars6,7,11–14. However, the interpretation of ^{142}Nd signatures is complicated by the presence of nucleosynthetic isotope variations between the terrestrial planets and meteorites. Such isotope anomalies arise from the heterogeneous distribution of presolar matter at the planetary scale, and have been documented for several elements15–18. Because different Nd isotopes have varying contributions from the *p*-, *s*- and *r*-processes of stellar nucleosynthesis (Extended Data Fig.1), the observed ^{142}Nd deficits in chondrites, relative to the accessible Earth, could in principle be nucleosynthetic in origin and, hence, unrelated to ^{146}Sm-decay8,16,19. Prior studies have identified nucleosynthetic Nd (and Sm) isotope anomalies in chondrites15,17 and their components20–23, but these effects do not seem to fully account for the observed ^{142}Nd deficits in chondrites. For instance, while the ^{142}Nd composition of carbonaceous chondrites can partly be attributed to an *s*-process deficit or a *p*-process deficit15,17, correction for these effects still leaves a ~20 ppm ^{142}Nd deficit compared to the accessible silicate Earth. This would be consistent with Nd isotope data for bulk ordinary chondrites, which also exhibit a ~20 ppm ^{142}Nd deficit, but do not seem to show resolvable nucleosynthetic Nd isotope anomalies15,17,24. Likewise, enstatite chondrites have ^{142}Nd deficit of ~10 ppm and also do not show clearly resolved nucleosynthetic Nd isotope anomalies24. Thus, prior studies concluded that the ^{142}Nd difference between chondrites and the accessible Earth largely reflects ^{146}Sm-decay and early Sm/Nd fractionation in the silicate Earth15,17,24. However, this interpretation remains uncertain because the available bulk chondrite data are of insufficient precision to detect collateral effects of nucleosynthetic heterogeneities on non-radiogenic Nd isotopes and, therefore, do not permit the reliable quantification of nucleosynthetic ^{142}Nd variations (Fig. 1).

Here we use high-precision Nd and Sm isotope measurements to better quantify nucleosynthetic Nd isotope variations between chondrites and the Earth, with the ultimate goal of determining the magnitude of any *radiogenic* ^{142}Nd difference between the accessible Earth and chondrites. We digested larger sample sizes (~2 g) than in most previous studies, allowing us to obtain higher precision Nd and Sm isotope data for a comprehensive set of meteorites including 18 chondrites, the ungrouped brachinite-like achondrite NWA 5363 and the Ca-Al-rich inclusion (CAI) A-ZH-5 from the Allende chondrite (Table 1). To evaluate the accuracy of our data, we processed the JNdi-1 standard and the terrestrial basalts BHVO-2 and BIR-1 through our full analytical procedures. Within uncertainty, the Nd and Sm isotope compositions of the processed and unprocessed standards (JNdi-1, AMES) are indistinguishable (Table 1; Fig. 2,3).

Most of the investigated chondrites tightly cluster around a 4.568 Ga ^{147}Sm-^{143}Nd isochron (Extended Data Fig. 2a). Only the EL6 chondrites Atlanta and Blithfield plot off the isochron, probably reflecting disturbance by late-stage impact events25; the ^{142}Nd data of these samples are, therefore, excluded from the following discussion. After correction of measured μ^{142}Nd (for definition of μ^{i}Nd and μ^{i}Sm see Table 1) values for ^{146}Sm-decay to the average chondritic ^{147}Sm/^{144}Nd = 0.1960 (ref. 1; Extended Data Table 1), the μ^{142}Nd values are tightly clustered for each chondrite group, where the enstatite chondrites define a mean μ^{142}Nd = -9±5 (95% conf.), the ordinary chondrites a mean μ^{142}Nd = -17±2, and the

Allende CV3 chondrite a mean μ^{142}Nd = -31±1. NWA 5363 exhibits a decay-corrected μ^{142}Nd of -16±7, similar to ordinary chondrites, while CAI A-ZH-5 has a decay-corrected μ^{142}Nd = -15±8, consistent with data for other Allende CAIs22.

In addition to variations in μ^{142}Nd, we find resolved systematic variations in non-radiogenic Sm and Nd isotopes (Table 1, Figures 1-3). Compared to previous studies we observe less scatter for each chondrite group, reflecting the long duration and high beam intensity of our measurements, resulting in more precisely defined average values for each group (Fig. 1). Plots of μ^{145}Nd and μ^{150}Nd versus μ^{148}Nd reveal positively correlated anomalies, with the enstatite chondrites being closest to the terrestrial value, followed by carbonaceous and ordinary chondrites, and then NWA 5363 (Fig. 2a,b). The meteorite samples plot along mixing lines between terrestrial Nd (*i.e.*, μ^{i}Nd=0) and pure *s*-process Nd, regardless of whether the *s*-process composition is derived from presolar SiC grains26, nucleosynthesis models27, or data for acid leachates of primitive chondrites20,21. Thus, the variability in non-radiogenic Nd isotopes among the meteorites reflects variable *s*-deficits relative to the Earth, consistent with inferences from other elements16,28,29.

The μ^{145}Nd, μ^{148}Nd and μ^{150}Nd anomalies of Allende are similar to those of ordinary and enstatite chondrites, although for most other elements nucleosynthetic anomalies are typically largest in carbonaceous chondrites16,18,28–30. The reason for the subdued Nd isotopic anomalies in Allende is the presence of CAIs, which host about half of the Nd and Sm in Allende31, and which, for these elements, are characterized by an *s*-excess and a *p*-deficit (Fig. 2,3). Mass balance calculations (Methods, Extended Data Table 2) indicate that a CAI-free carbonaceous chondrite composition would have μ^{145}Nd, μ^{148}Nd and μ^{150}Nd values of 27±14, 39±28, and 56±41; these anomalies are larger than those of ordinary and enstatite chondrites and thus imply that prior to addition of CAIs, carbonaceous chondrites had a significant *s*-deficit (Fig. 2a,b). This interpretation is consistent with Sm isotope data for Allende and other carbonaceous chondrites, because the calculated CAI-free composition of these chondrites also shows an *s*-deficit (Fig. 2c, Extended Data Fig. 3). Thus, the displacement of the carbonaceous chondrites from the *s*-deficit line defined by ordinary and enstatite chondrites reflects the admixture of CAIs to carbonaceous chondrites. Note that, for ordinary and enstatite chondrites, the effects of admixing CAIs are probably insignificant at the ~2 ppm level (Extended Data Table 2), and that the expected *s*-process Sm isotope anomalies (<10 μ^{144}Sm and > –20 μ^{148}Sm) for these two groups of chondrites are too small to be resolvable with the analytical precision of our Sm isotope measurements.

Using the information gained from the non-radiogenic isotopes, we can now assess the effect of nucleosynthetic anomalies on μ^{142}Nd. The bulk meteorite data show inverse correlations between μ^{142}Nd and μ^{145}Nd, μ^{148}Nd, μ^{150}Nd and μ^{144}Sm (Fig. 3), which are consistent with the co-variations expected from a heterogeneous distribution of *s*-process isotopes. Enstatite and ordinary chondrites, as well as NWA 5363, plot on mixing lines between terrestrial and *s*-process Nd. The Allende CV3 chondrite is displaced from these correlations due to the admixture of CAIs, and a calculated CAI-free carbonaceous chondrite composition plots on the *s*-mixing line defined by the other meteorites (Fig. 3).

The slopes obtained from linear regressions of the bulk meteorites (excluding Allende) are in good agreement with those calculated for mixing lines between terrestrial and *s*-process Nd, regardless of which estimate for the *s*-process composition is used20,21,26,27 and whether or not the calculated CAI-free carbonaceous chondrite composition and the processed standards are included in the regressions (Extended Data Figure 4). The intercept values obtained from the regressions can thus be used to determine μ^{142}Nd values corrected for *s*-process heterogeneity. For all regressions the intercept values are indistinguishable from each other and average at a value of *ca*. –5 ppm relative to the JNdi-1 standard (Extended Data Table 3). Alternatively, μ^{142}Nd values corrected for nucleosynthetic anomalies can be calculated for each meteorite group separately, using their measured μ^{145}Nd, μ^{148}Nd and μ^{150}Nd values combined with the slopes of the *s*-mixing lines. Regardless of which *s*-process mixing relationships are applied, the calculated $\mu^{142}Nd_{s\text{-corrected}}$ values are all mutually consistent and indistinguishable from each other (Extended Data Table 3), resulting in an average $\mu^{142}Nd_{s\text{-corrected}}$= –5±2 ppm. Although this value is slightly negative, it is within the long-term ~±5 ppm reproducibility of the JNdi-1 standard. When the regressions and corrections are calculated relative to the mean Nd isotope composition measured for the processed terrestrial standards, $\mu^{142}Nd_{s\text{-corrected}}$ reduces to –2±2 ppm (Extended Data Table 3). We conclude that after correction for nucleosynthetic Nd isotope heterogeneity, the ^{142}Nd compositions of chondrites and the accessible silicate Earth are indistinguishable at the current level of analytical precision of ~5 ppm.

The lack of a resolved radiogenic ^{142}Nd difference between chondrites and the accessible silicate Earth supports the long-standing paradigm of a chondritic Sm/Nd for the bulk Earth and requires revision of conclusions from several prior studies about the early differentiation, composition, structure, and heat budget of the Earth. These prior studies interpreted the ^{142}Nd offset between chondrites and terrestrial samples to result from ^{146}Sm-decay and an early global Sm/Nd fractionation in the Earth's mantle3,6,7,9,10. However, our results demonstrate that chondrites and the accessible Earth have indistinguishable radiogenic ^{142}Nd compositions and, therefore, remove the evidence for an early global silicate differentiation of the Earth. This revision indicates that the hidden, enriched reservoir hypothesized in earlier studies3,6,9,10 does not exist. Moreover, our results rule out the extensive loss of early-formed crust by collisional erosion3,7,9, because otherwise the bulk silicate Earth would not have a chondritic Sm/Nd. Finally, the evidence for chondritic Sm/Nd in the bulk Earth implies chondritic abundances of other refractory elements, including the heat-producing elements U and Th. Thus, the total radiogenic heat generated over Earth's history is almost a factor of two higher than estimated recently for a non-chondritic composition of the Earth9.

Our results demonstrate that chondrites are the most appropriate proxy for the elemental composition of the Earth. However, they also highlight that chondrites cannot be the actual building blocks of the Earth, because they are deficient in a presolar component containing *s*-process matter. The *s*-process deficit becomes larger in the order enstatite < ordinary < carbonaceous chondrites, indicating that the distribution of presolar matter in the solar protoplanetary disk varied as a function of heliocentric distance, or changed over time. For instance, the nucleosynthetic isotope heterogeneity within the disk may reflect a different magnitude in the thermal processing of stellar-derived dust, imparting isotopic heterogeneity

on an initially homogeneous disk, but could also reflect distinct compositions of infalling molecular cloud material added to the disk at different times18,28–30. Either way, the increasing deficit in *s*-process matter with increasing heliocentric distance provides a new means for identifying genetic relationships among planetary bodies. For instance, Mars formed at a greater heliocentric distance than Earth and should, therefore, be characterized by an *s*-process deficit, possibly similar to those observed for enstatite and ordinary chondrites. Thus, high-precision Nd isotopic data for martian meteorites will make it possible to determine the distinct sources of the building materials of Earth and Mars. This information is not only critical for dating the differentiation of Mars13, but also for testing models of terrestrial planet formation.

Methods

Samples

To avoid potential artifacts associated with incomplete dissolution of refractory presolar components and to minimize potential disturbances through terrestrial alteration, only equilibrated chondrites (petrologic classes 4-6; except the CV3 Allende) from observed falls were selected for this study. Equilibrated chondrites are devoid of presolar grains, because these components were destroyed during thermal metamorphism on the meteorite parent body32; for Allende (3.2 to >3.6 metamorphic grade), which may contain trace amounts of presolar grains32, no difference in Nd isotopic composition was observed between table-top acid-digested, bomb digested and alkali-fused samples6,17, indicating that for this meteorite all Nd carriers are accessed by standard acid digestion. Our sample set includes eleven ordinary chondrites (six H, two L and three LL), six enstatite chondrites (three EL and three EH), the carbonaceous chondrite Allende, and the brachinite-like achondrite NWA 5363, which is a melt-depleted ultramafic sample from a partially differentiated asteroid33. This brachinite-like sample was added to the study because of its unique isotope anomalies: while the O and Ni isotopic compositions of NWA 5363 are indistinguishable from the terrestrial composition, it exhibits nucleosynthetic isotope anomalies in Ti, Ca, Mo and Ru that are more akin to ordinary chondrites34. In addition to bulk meteorites, we analyzed the Ca-Al-rich inclusion (CAI) A-ZH-5 from the Allende chondrite and, to evaluate the accuracy of our analytical methods, we also processed the JNdi-1 standard, as well as the terrestrial basalt standards BHVO-2 and BIR-1 through our full analytical procedures.

Sample preparation and chemical separation of Nd and Sm

Meteorite pieces were cleaned with abrasive paper, ultrasonicated in methanol, and subsequently crushed to a fine powder in an acid-cleaned agate mortar exclusively used for meteorite work at the Origins Lab, Chicago. For each analysis about 2 g of meteorite powder was digested in a HF-HNO_3-$HClO_4$ mixture and *aqua regia* in 90 ml Savillex teflon vials for about 10 days on a hotplate at 170 °C. After several dry-downs, ultrasonication and redissolution steps in *aqua regia* and HCl, the samples were redissolved in HCl and, once a clear solution was obtained, a ~5% aliquot was taken for Sm and Nd concentration measurements by isotope dilution.

Chemical procedures for Sm and Nd concentration measurements—The 5% aliquots were sent from the Origins Lab to LLNL, where they were equilibrated with a ^{149}Sm-^{150}Nd mixed isotopic tracer. Rare earth elements (REE) were purified from the matrix of these aliquots using 2 mL BioRad columns filled with AG50-X8 (200-400 mesh) resin and 2 N and 6 N HCl. The REE were further purified using 150µl Teflon columns with RE-Spec resin and 1N and 0.05N HNO_3. Samarium and Nd were purified from other REE using 15 cm glass columns, Ln-Spec resin, and 0.25 N and 0.60 N HCl. Total blanks of the isotope dilution procedures were 25 pg of Nd and 8 pg of Sm, resulting in Nd and Sm sample-to-blank ratios greater 1500 for all but one sample. The blank corrections resulted in shifts in the $^{147}Sm/^{144}Nd$ ratios that were less than 0.003% and thus significantly smaller than the typical uncertainty of 0.1% associated with the isotope dilution measurements. For NWA 5363, the Nd and Sm sample-to-blank ratios were 751 and 760, respectively, and thus required a blank correction of 0.13% on the Nd and Sm concentrations (*e.g.* the reported 0.112 ppm Nd abundance was corrected by 0.00015 ppm). The blank correction is reflected in the larger uncertainty of 0.2% on the $^{147}Sm/^{144}Nd$ of NWA 5363.

Chemical procedures for Sm and Nd isotope composition measurements—After aliquoting, the remaining ~95% of the sample solution was reduced and HNO_3 was added. The REE cut of CAI A-ZH-5 that was obtained in a previous study35 (where the digested sample was processed through an anion exchange chromatography to separate Ti, Zr, Hf, W and Mo from the matrix; for details see ref. 35) was added to the project at this point. After additional dry-downs in aqua regia and HNO_3, samples were redissolved in ~35 ml of 3 M HNO_3 and 350 mg of H_3BO_3 was added before the solutions were centrifuged. A fine-grained black low-density residue, probably carbon-based, was present for some of the chondrites at this point and was discarded; note that since we analyzed equilibrated chondrites, this C-bearing phase does not contain presolar material and therefore does not influence the Nd isotopic composition of the non-radiogenic isotopes. Furthermore, significant alteration of the Sm/Nd ratios or the radiogenic Nd isotopic signatures of the samples by this material is also excluded, given the very good agreement of our decay-corrected ^{142}Nd and ^{143}Nd data with previous studies (Fig. 1; Extended Data Fig. 2). After centrifugation, the solutions were loaded onto two 2 ml Eichrom TODGA ion exchange columns stacked on each other, on which the REE were separated from the matrix elements36. To further purify the REE cut, the separation was repeated using a 1×2 ml TODGA column. Separation of Sm and Nd from interfering REEs was accomplished with 0.2×25 cm long quartz columns with AG50W-X8 (NH_4^+ form, pH~7) as stationary phase and 0.2 M alpha-hydroxyisobutyric acid (pH adjusted to 4.6) as the fluid phase. The Sm and Nd cuts were passed twice over this column at the University of Chicago and were then sent to LLNL. Neodymium was further purified at LLNL using 0.2 M alpha-hydroxyisobutyric acid adjusted to a pH of 4.40 on pressurized quartz glass columns loaded with AG50W-X8 (NH_4^+ form) resin. Neodymium was separated from the alpha-hydroxyisobutyric acid using 2 ml columns loaded with AG50W-X8 (200-400 mesh) resin using water, 2 N HCl, and 6 N HCl. The yields of the chemical procedure were determined by ICP-MS on small aliquots of the processed Nd and Sm cuts and ranged between 62 and 95 % for Nd (with a mean yield of 80%) and 56 and 98 % for Sm (with a mean yield of 75%). The variable yields do not have any noticeable influence on the measured Nd and Sm isotopic compositions. This is

indicated by the fact that (i) several samples processed multiple times displayed variable yields, but had very homogeneous isotopic compositions, and (ii) the terrestrial rock standards passed through the chemistry have indistinguishable compositions from the unprocessed standard. These observations further suggest that either the exponential law is well-suited to correct any yield-related induced mass-dependent isotope variations, or, that the sample loss is associated with processes that do not induce mass-dependent fractionation effects, *e.g.*, pipetting of the samples on the columns or loss of dry sample material from the beakers by static effects. The latter erratic losses seem to be the most likely explanation for the variable yields, which vary in a non-systematic way within a chemical campaign and among multiple digestions of the same meteorites. The procedural blanks associated with Nd and Sm isotope composition measurements were 50 and 12 pg respectively, and thus contributed negligibly (<0.03 % of total analyte) to the isotope compositions of the samples, requiring no corrections to be made.

Procedures of Nd and Sm isotope measurement by TIMS

The Nd isotope compositions were analyzed using a ThermoScientific Triton thermal ionization mass spectrometer at LLNL. Neodymium was loaded on zone-refined Re filaments in 2 N HCl and analyzed as Nd^+ using a second Re ionization filament. Isotope ratios were measured using a two mass-step procedure that calculates $^{142}Nd/^{144}Nd$ and $^{148}Nd/^{144}Nd$ dynamically, while measuring the other Nd isotopes statically following a modified version of previously established procedures17. The cup configuration of line 1 and 2 are: L3=^{142}Nd, L2=^{143}Nd, L1=^{144}Nd, C=^{145}Nd, H1=^{146}Nd, H2=^{148}Nd, H3=^{149}Sm, H4=^{150}Nd and L3=^{140}Ce, L2=^{141}Pr, L1=^{142}Nd, C=^{143}Nd, H1=^{144}Nd, H2=^{146}Nd, H3=^{147}Sm, H4=^{148}Nd, respectively. Individual mass spectrometer runs consisted of 540 ratios of 8 second integrations. The dynamic $^{142}Nd/^{144}Nd$ ratio is calculated from $^{142}Nd/^{144}Nd$ measured in cycle 2 normalized to $^{146}Nd/^{144}Nd$ measured in cycle 1, whereas the dynamic $^{148}Nd/^{144}Nd$ ratio is calculated from the $^{148}Nd/^{146}Nd$ ratio measured ratio in cycle 1 normalized to $^{146}Nd/^{144}Nd$ measured in cycle 2. The $^{143}Nd/^{144}Nd$ ratio is calculated from the average of the 1080 ratios of data collected in cycles 1 and 2. The $^{145}Nd/^{144}Nd$ ratio represents the average of 540 ratios collected in cycle 1. Most samples were run at least twice from the same filaments. Signal sizes varied from $^{144}Nd = 3.2\times10^{-11}$ to 5.4×10^{-11} A, with most averaging in excess of 4.3×10^{-11} A. Fractionation was corrected assuming $^{146}Nd/^{144}Nd = 0.7219$ using the exponential law. The Nd isotope data were acquired in three measurement campaigns that were separated by a cup exchange and maintenance work on the Triton. To avoid any bias which might have been introduced by these events, the data obtained in each of the campaigns were normalized to the mean JNdi-1 composition measured in the respective campaign (Supplementary Information). The external reproducibility of the standard (2 s.d.) for $^{142}Nd/^{144}Nd$, $^{145}Nd/^{144}Nd$, $^{148}Nd/^{144}Nd$, and $^{150}Nd/^{144}Nd$ in campaign 1, 2 and 3 are 5, 9, 3, and 24 ppm, 6, 6, 7 and 24 ppm and 8, 13, 15 and 31 ppm, respectively. Table 1 presents average values of multiple measurements from the same filament. The associated uncertainties represent the external reproducibility (2 s.d.) of the standard during that campaign, or the uncertainty of the sample measurements ($2\sigma_{mean}$), which were larger than the external reproducibility of the standard (3 ppm) for some of the $^{148}Nd/^{144}Nd$ sample runs in campaign 1. Interferences from Ce and Sm are

monitored at ^{140}Ce and ^{149}Sm and are presented in Table 1 of the Supplementary Information.

Samarium was loaded in 2 N HCl onto a zone-refined Re filament and analyzed as Sm^{+} using double Re filaments. All Sm isotopes, along with interferences from Nd (measured as ^{146}Nd) were measured statically for 200 ratios of 8 seconds integration each. Instrument fractionation was corrected assuming $^{147}Sm/^{152}Sm = 0.56803$ using the exponential law. The cup configuration for Sm isotope composition measurements is: L4=^{144}Sm, L3=^{146}Nd, L2=^{147}Sm, L1=^{148}Sm, C=^{149}Sm, H1=^{150}Sm, H2=^{152}Sm, H3=^{154}Sm, H4=^{155}Gd. Sample measurements consisted of one to three static runs from the same filament, depending on the amount of Sm available, and were obtained at 1-2×10^{-11} A ^{149}Sm. The data were acquired in three campaigns and are given in the Supplementary Information. Samarium isotope anomalies were calculated relative to the mean composition of the AMES Sm standard analyzed in each campaign (Supplementary Information). The external reproducibility of the standard for $^{144}Sm/^{152}Sm$, $^{148}Sm/^{152}Sm$, $^{149}Sm/^{152}Sm$, $^{150}Sm/^{152}Sm$ and $^{154}Sm/^{152}Sm$ in campaign 1, 2 and 3 are 22, 12, 14, 12 and 18 ppm, 43, 10, 10, 18 and 13 ppm, and 38, 10, 12, 13 and 11 ppm, respectively. Table 1 presents average values of the multiple measurements run from the same filament, and the reported uncertainties are 2 s.d. of the standard.

The Nd and Sm concentrations were determined using a ThermoScientific TIMS in static mode. Measurements consisted of 200 cycles with 8 second integration time each. Concentration data and $^{147}Sm/^{144}Nd$ ratios are given in Table 3 of the Supplementary Information. Note that the nucleosynthetic anomalies measured here have no significant effect on the accuracy and precision of the Sm and Nd concentration measurement (the minimum variation in the Sm and Nd isotopic compositions that would be required to shift the $^{147}Sm/^{144}Nd$ ratios beyond uncertainty are 270 μ^{i}Sm and 560 μ^{i}Nd units, respectively; and thus significantly larger than the deviations we observed).

Isotopic mass-balance between CAIs and Allende

Calcium-aluminum-rich inclusions found in carbonaceous chondrites are considered the oldest surviving objects to have formed in the solar nebula, presumably by condensation from nebular gas. They often exhibit isotopic anomalies significantly different than their chondrite host rocks16,18,22,23,37, strongly suggesting that they are not genetically related to the reservoir from which the other chondrite components (namely chondrules and matrix) originated. The Nd and Sm isotopic composition of bulk carbonaceous chondrites is thus most likely influenced by CAIs, especially since the (light) rare earth elements in these objects are enriched relative to the host rocks (*e.g.*, up to ~20× for the CV chondrites, up to ~100× in CM chondrites).

Indeed, our measurements imply a strong control of CAI material on the Nd and Sm isotope composition of bulk carbonaceous chondrites, because our Allende data as well as literature data of carbonaceous chondrites are displaced towards the CAI composition in μ^{x}Nd *vs.* μ^{y}Nd, μ^{x}Nd *vs.* μ^{y}Sm and μ^{x}Sm *vs.* μ^{y}Sm diagrams (Fig. 2,3; Extended Data Fig. 3).

In order to quantify the effect of CAIs on the Allende composition and characterize the composition of the CAI-free carbonaceous chondrite source reservoir we performed an isotopic mass balance calculation. For Nd this has the form

$$Nd_{Allende} = X Nd_{source} + (1 - X) Nd_{CAI} \quad (1)$$

where $Nd_{Allende}$ is the concentration of Nd in Allende, which is given by the sum of Nd in the carbonaceous chondrite source reservoir (Nd_{source}) and the Nd contributed by the CAIs (Nd_{CAI}) and X is the fraction of non-CAI material in Allende.

For the isotopic composition we can likewise write

$$\mu^x Nd_{Allende} Nd_{Allende} = X \mu^x Nd_{source} Nd_{source} + (1 - X) \mu^x Nd_{CAI} Nd_{CAI} \quad (2)$$

Using the isotopic compositions measured for Allende (this study) and Allende CAIs (mean value of 11 CAIs reported in ref. 22) and 3% CAIs in Allende38, and a mean Nd concentrations of 0.967 and 14 ppm for Allende and Allende CAIs31, we can solve for the unknown concentration and isotopic composition of the CAI-free material according to:

$$Nd_{source} = \frac{Nd_{Allende} - (1 - X) Nd_{CAI}}{X} \quad (3)$$

and

$$\mu^x Nd_{source} = \frac{\mu^x Nd_{Allende} Nd_{Allende} - (1 - X) \mu^x Nd_{CAI} Nd_{CAI}}{Nd_{Allende} - (1 - X) Nd_{CAI}} \quad (4)$$

The uncertainty on $\mu^x Nd_{source}$ is mainly determined by the uncertainties on the measured isotopic compositions of Allende and the CAIs and was calculated by propagating them according to:

$$\sigma^2_{\mu^x Nd_{source}} = \left(\frac{\partial F_{(\mu^x Nd_{source})}}{\partial^x Nd_{Allende}} \right)^2 \sigma^2_{\mu^x Nd_{Allende}} + \left(\frac{\partial F_{(\mu^x Nd_{source})}}{\partial^x Nd_{CAI}} \right)^2 \sigma^2_{\mu^x Nd_{CAI}} \quad (5)$$

Equivalent equations can be written for Sm. The mass-balance was performed using mean Sm concentrations of 0.313 and 4.54 for Allende and the CAIs, respectively (*i.e.*, with chondritic Sm/Nd ratios for both objects). All input parameters and the resulting composition of the carbonaceous chondrite source reservoir are also given in the Extended Data Table 2.

The Nd and Sm mass-balance calculations indicate that the CAI-free carbonaceous chondrite source reservoir is characterized by a significant *s*-deficit relative to the Earth and the other

chondrites, in both, Nd and Sm isotopes. This is consistent with information derived from other isotope systems (*e.g.*, Sr, Zr, Mo, Ru) where carbonaceous chondrites are characterized by the largest *s*-deficits relative to the Earth, followed by ordinary and enstatite chondrites16,28,29,39. We note that carbonaceous chondrite data obtained in previous studies15,17 also plot along the mass-balance mixing relation between CAIs and a CAI-free carbonaceous chondrite source. This implies that (i) the isotopic composition of the other carbonaceous chondrites are also influenced by CAI-like material, and (ii) that they derive from a common *s*-depleted reservoir. The fact that some of the other carbonaceous chondrites also plot on the mixing line close to the bulk Allende values, despite containing fewer CAIs than CV chondrites, might be due to the higher REE enrichments in these non-CV CAIs (*e.g.*, hibonites in CM chondrites) or the fact that CAI-like material is not present in the form of well-defined inclusions but could be dispersed in the matrix in the form of small dust grains partially altered by parent-body metamorphism. Since no Sm and Nd isotope data of non-CV carbonaceous chondrite CAIs are available, one can only speculate whether or not these CAIs also might carry larger nucleosynthetic Sm and Nd anomalies than Allende CAIs.

In principle, the Nd and Sm isotope compositions observed in ordinary and enstatite chondrites could also be influenced by CAIs. However, petrographic and chemical investigations imply that CAI-like material in these chondrite types is extremely rare38,40–42; and no Sm and Nd isotope data of these objects are available. Nevertheless, the effect of CAIs on the measured bulk Nd and Sm isotope composition of enstatite and ordinary chondrites is estimated to be no larger than 2 ppm for Nd and 5 ppm for Sm, respectively (Extended Data Table 2). This calculation assumes that the CAI-like material in ordinary and enstatite chondrites has a maximum REE enrichment of 50×CI chondritic and an isotopic composition like normal Allende CAIs, and that the maximum CAI abundance in these chondrites is 0.05%. Given the small effects, we have omitted any correction of our measured data. However, we note that any such correction would result in slightly larger anomalies in non-radiogenic Nd isotopes and thus a higher $\mu^{142}Nd_{s\text{-corrected}}$, *i.e.*, an even better agreement between the nucleosynthetic anomaly-corrected $\mu^{142}Nd$ of meteorites and the accessible Earth.

CAIs do not only exhibit isotope anomalies in Nd and Sm, but also for many other elements16,18,22,30,37. In order to explore the collateral effects of the mass-balance between CAIs and Allende defined above for Nd and Sm on other isotope systems, we also applied it to Ca, Ti, Cr, Ni, Sr, Zr, Mo and Ba. The input parameters and results are given in the Extended Data Table 4. Compared to the results from Nd and Sm, the isotopic compositions calculated for the CAI-free carbonaceous chondrite source reservoir for Ca, Ti, Cr, Ni, Sr, Zr, Mo and Ba are not very different from the bulk Allende values (the most significant change is the reduction of the $\mu^{50}Ti$ anomaly from 365±34 for bulk Allende to 221±46 for the CAI-free component, consistent with the measured value (189±6) of a CAI-free Allende sample18). This is explained by the fact that the chemical enrichment of these elements in the CAIs relative to the host-rock are not as strong as for Nd and Sm, and that the anomalies in the CAIs and bulk Allende are less disparate than for Nd and Sm. In other words, the CAIs have a less significant influence on the bulk Allende isotopic composition for Ca, Ti, Cr, Ni, Sr, Zr, Mo and Ba, than they have for Nd and Sm. We note, however, that

the calculated CAI-free Allende compositions for Sr, Zr, and Mo isotope anomalies are fully consistent with the inferences made above from Nd and Sm, *i.e.*, the formation of the carbonaceous chondrites from a nebular reservoir depleted in *s*-process material relative to Earth.

Extended Data

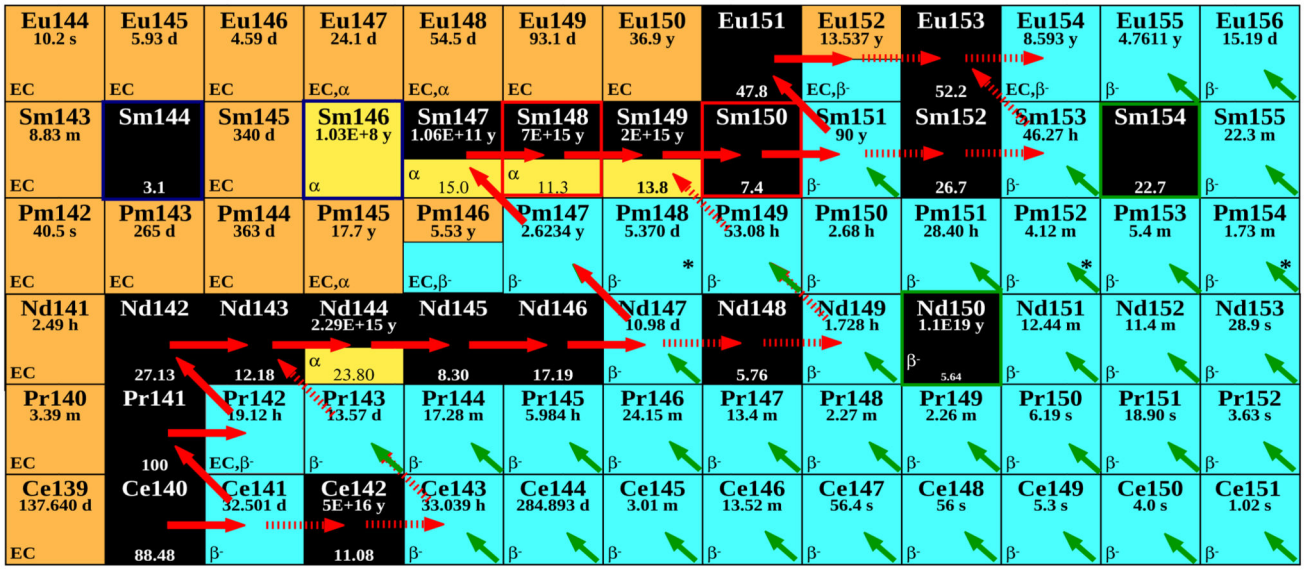

Extended Data Fig. 1. Chart of the nuclides in the Ce-Nd-Sm-Gd mass-region (upper panel) and plots illustrating the effect of nucleosynthetic anomalies on the measured Nd and Sm isotope compositions (lower panels).

Stable isotopes and their solar abundances are in black boxes on the chart, short-lived isotopes and their half-lives in colored boxes; blue (β^- unstable), orange (electron capture) and yellow (α-decay). Solid red arrows mark the main path of *s*-process, dashed red arrows mark minor *s*-process branches, and green arrows indicate the decay path of *r*-process nucleosynthesis. ^{148}Sm and ^{150}Sm are produced only by the *s*-process, ^{150}Nd and ^{154}Sm

Europe PMC Funders Author Manuscripts

Europe PMC Funders Author Manuscripts

only by the *r*-process, and ^{144}Sm and ^{146}Sm are *p*-process only isotopes. Lower panels show expected μ^{i}Nd and μ^{i}Sm anomaly patterns for a *p*-process deficit (purple), a *s*-process deficit (red) and a *r*-process excess (green) for internal normalization to ^{146}Nd/^{144}Nd and ^{152}Sm/^{147}Sm, respectively calculated using stellar model abundances27.

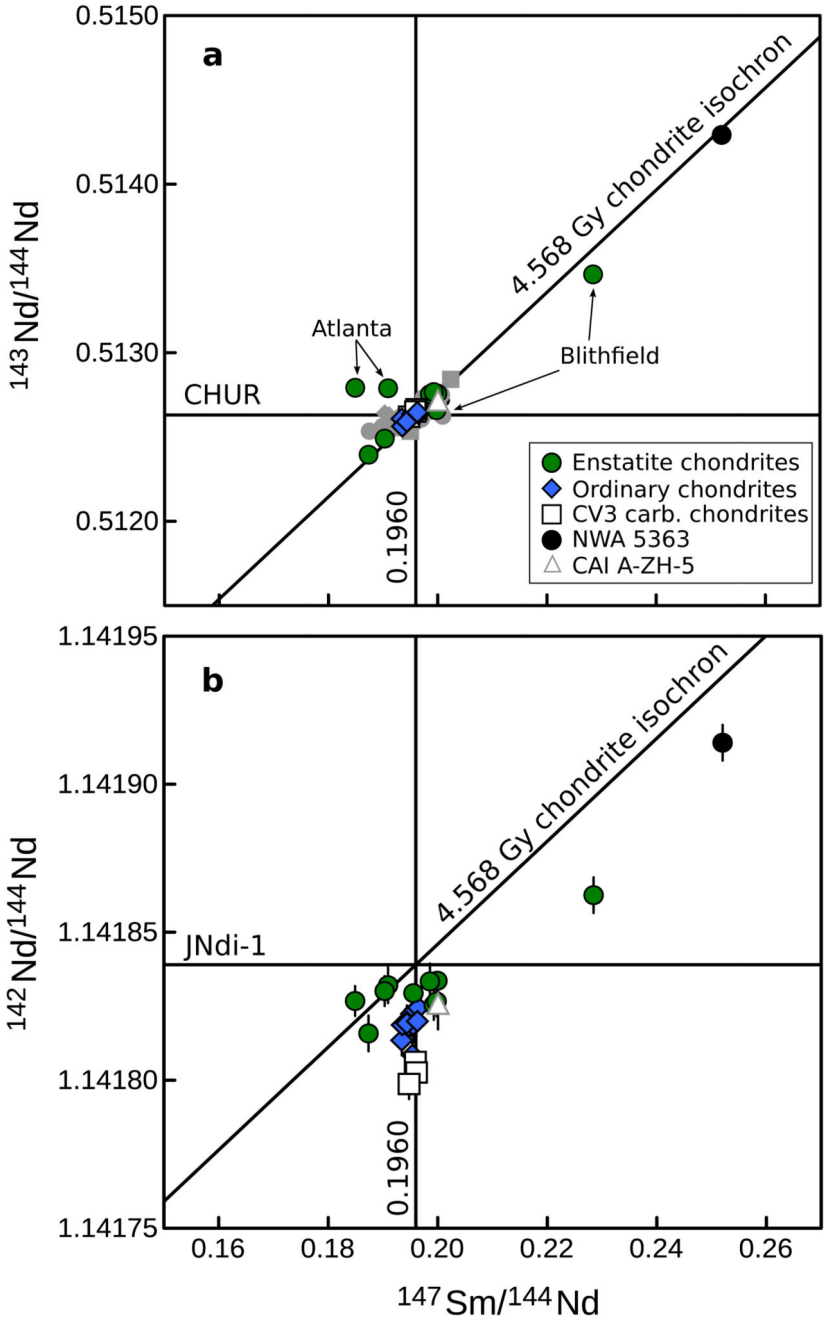

Extended Data Fig. 2. Sm/Nd isochron diagrams of measured meteorite samples.

a, For ^{143}Nd/^{144}Nd all but the disturbed Atlanta and Blithfield chondrites cluster in a narrow range around a 4.568 Gyr chondrite isochron, consistent with literature data (grey). **b,**

Europe PMC Funders Author Manuscripts

For $^{142}Nd/^{144}Nd$, the meteorite data mostly fall below a 4.568 Ga isochron constructed through the accessible Earth value and only poorly correlate with Sm/Nd, indicating that besides Sm/Nd fractionation and ^{146}Sm-decay, other processes are responsible for setting the $^{142}Nd/^{144}Nd$ of meteorites.

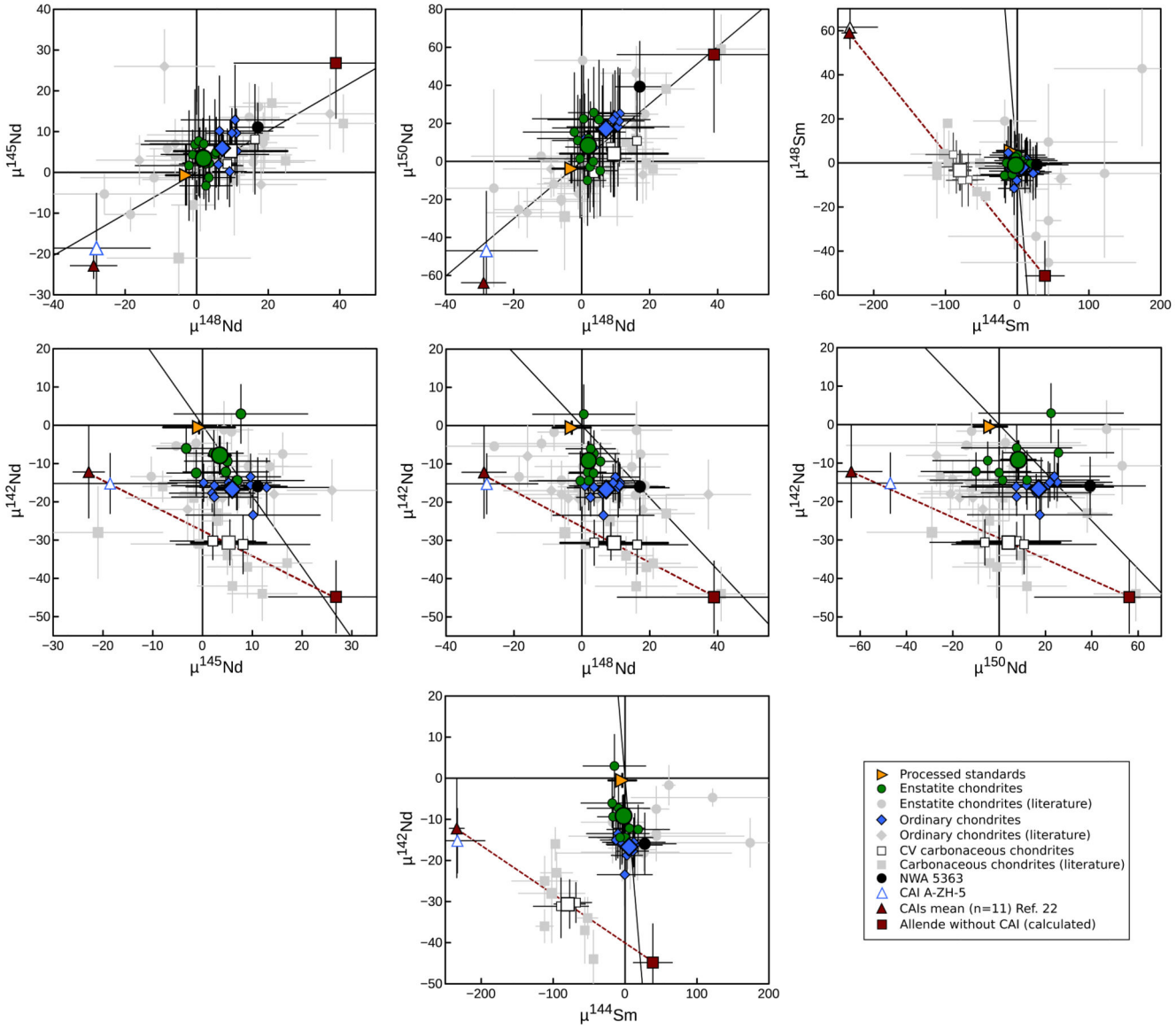

Extended Data Fig. 3. Comparison of Nd and Sm isotope data obtained here and literature values.

The new data agrees with literature data (in grey), but show less scatter, facilitating the calculation of precise group averages. Of note, uncertainties shown for our measurements represent external reproducibility (2s.d. of the standards), while uncertainties for the literature values are internal 2s.e. of the measurements. Solid line denotes mixing of *s*-model prediction27 with the terrestrial composition. Dashed line is mixing line between CAIs and CAI-free carbonaceous chondrite source reservoir as calculated by isotopic mass balance.

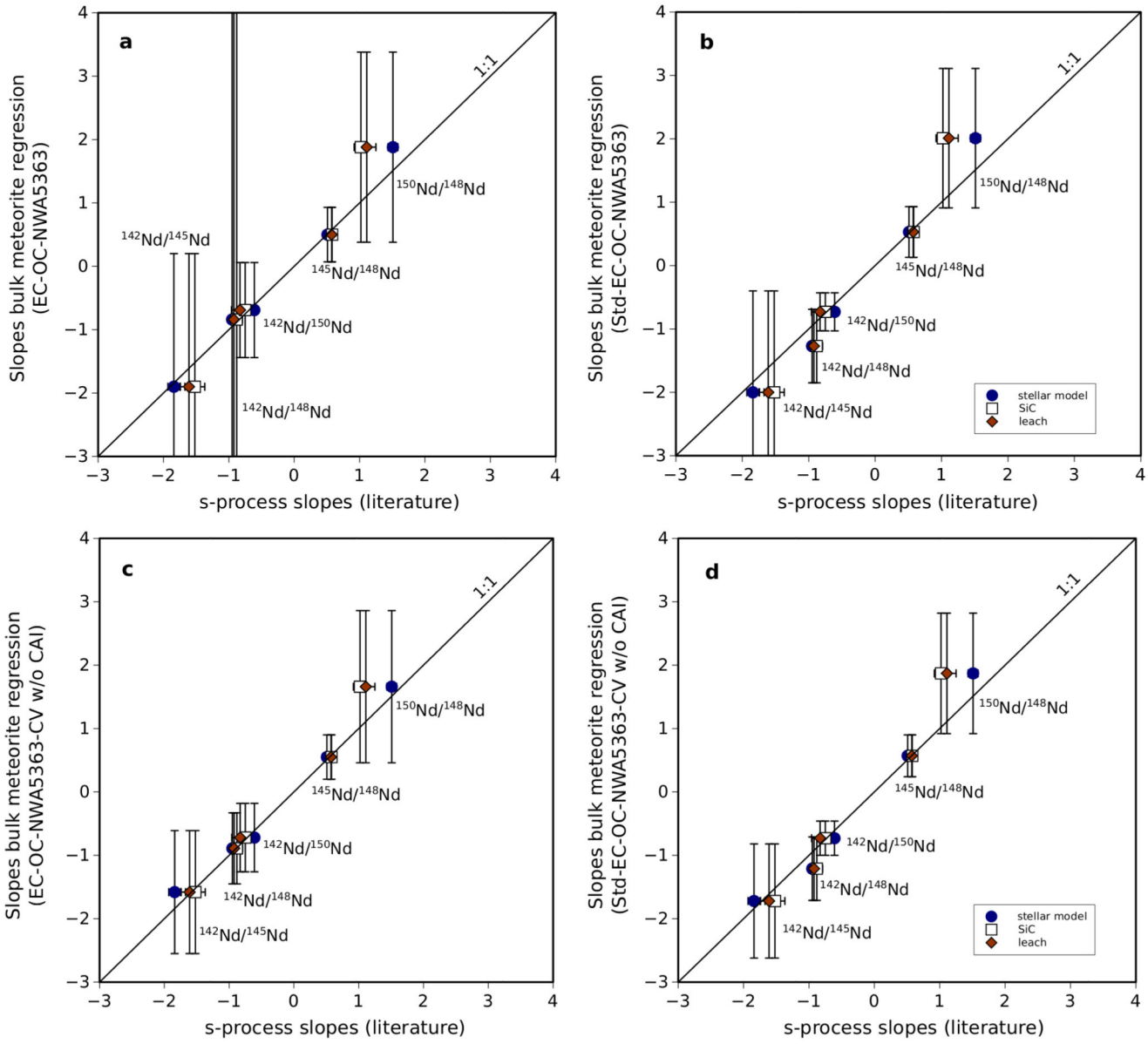

Extended Data Fig. 4. Comparison of slopes obtained from bulk meteorite anomaly data regressions and slopes obtained from *s*-process modeling27, SiC grain data26 and chondrite leachate data20,21.

a, Slopes from regression of EC, OC, NWA 5363 data; **b,** same as before but including the processed standard data in the regression. **c,** Slopes from regression of EC, OC, NWA 5363 values and calculated CAI-free Allende point (CV w/o CAI); **d,** same as before but including the processed standard data in the regression. Within uncertainties, the slopes from the bulk meteorite regressions are indistinguishable from the slopes from the literature data, no matter which samples are used in the regressions. This implies that the Nd isotope variations in ECs, OCs, NWA 5363 and the CAI-free carbonaceous chondrite source are due to *s*-process heterogeneities. All regressions were performed using ISOPLOT. The slopes and μ^{142}Nd intercepts of the regressions are also given in Extended Data Table 3.

Europe PMC Funders Author Manuscripts

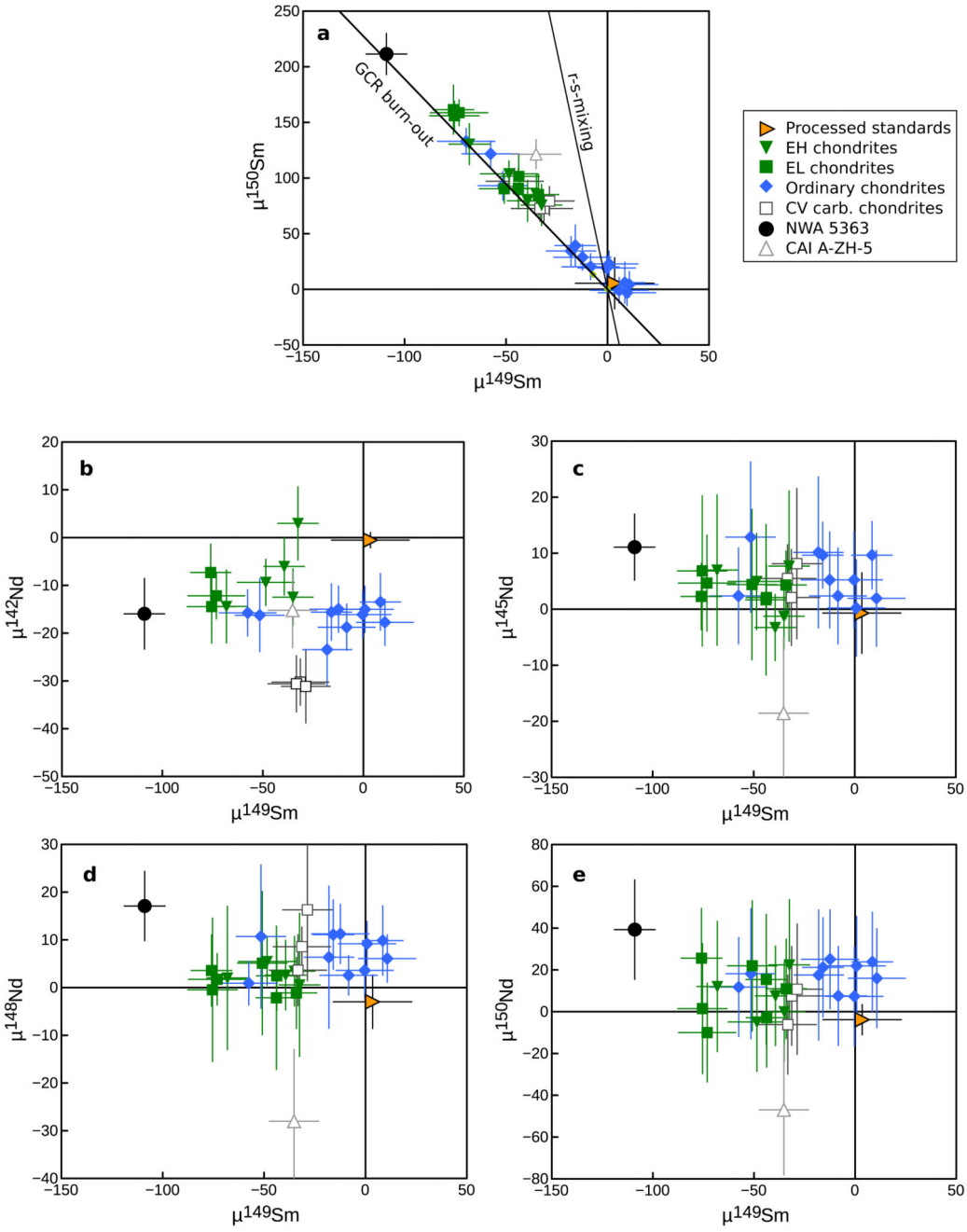

Extended Data Fig. 5. Effects of meteoroid exposure to galactic cosmic rays (GCR) on the Sm and Nd isotope compositions.

a, Meteorites of this study show correlated $\mu^{149}Sm$ and $\mu^{150}Sm$ anomalies consistent with GCR exposure. Such reactions can also alter the Nd isotope signatures of planetary materials43. However, given the much smaller neutron capture cross sections of the Nd isotopes relative to ^{149}Sm, any effect of GCR on $\mu^{142}Nd$ is <1ppm. **b-e,** Within a given meteorite group no obvious correlations are seen in $\mu^{i}Nd$ versus $\mu^{149}Sm$, indicating the absence of significant GCR effects on the Nd isotope data.

Europe PMC Funders Author Manuscripts

Extended Data Table 1

Measured and calculated $^{147}Sm/^{144}Nd$ and $\mu^{142}Nd$ values.

In order to investigate the effect of nucleosynthetic anomalies on $\mu^{142}Nd$ with high precision, the measured $\mu^{142}Nd$ values of the meteorites first need to be corrected for ^{146}Sm decay to a constant $^{147}Sm/^{144}Nd = 0.1960$ (ref. 1) and assuming a common 4.568 Gy evolution with a solar system initial $^{146}Sm/^{144}Sm = 0.00828\pm0.00044$ (ref. 23). This can be done either by using the measured $^{147}Sm/^{144}Nd$ values ('$\mu^{142}Nd$ corrected 1'), or the $^{147}Sm/^{144}Nd$ values are first calculated from the measured $^{143}Nd/^{144}Nd$, a chondritic $^{143}Nd/^{144}Nd = 0.512630$ (ref. 1) and a $\lambda^{147}Sm = 6.539\times10^{-12}$ ('$\mu^{142}Nd$ corrected 2'). The latter method is insensitive to recent changes in the Sm/Nd ratio, *e.g.*, through terrestrial weathering or incomplete spike-sample equilibrium, while the former is less model dependent. Within uncertainties, both correction methods yield indistinguishable $\mu^{142}Nd$ values and with the exception of Abee and the radiogenic NWA 5363, these values are also indistinguishable from the measured values. For both corrections the uncertainties on the initial $^{146}Sm/^{144}Sm$, $^{147}Sm/^{144}Nd$, and the measured $\mu^{142}Nd$ were propagated, but a significant change is only observed for NWA 5363, whose decay correction (83 ppm) changed the uncertainty from ±6 to ±7.5 ppm. Data for the Atlanta and Blithfield EL6 chondrites are excluded (italic) due to their disturbed Sm/Nd systematics.

Sample	Type	$^{147}Sm/^{144}ND$ measured	2se	$\mu^{142}Nd$ measured	2sd	$\mu^{142}Nd$ corrected 1	2sd	$^{143}Nd/^{144}Nd$ measured	2sd	$^{147}Sm/^{144}Nd$ calculated	2sd	$\mu^{142}Nd$ corrected 2	2sd
Hvittis (1)	EL6	0.1999	0.0002	-6	5	-12	5	0.5127579	0.0000027	0.2003	0.0001	-13	5
Hvittis (2)	EL6	0.1986	0.0002	-3	6	-7	6	0.5127533	0.0000060	0.2001	0.0002	-10	6
Hvittis (3)	EL6	0.1993	0.0002	-10	8	-14	8	0.5127663	0.0000051	0.2005	0.0002	-16	8
Atlanta (1)	EL6	*0.1909*	*0.0002*	*-5*	*6*	*3*	*6*	*0.5127888*	*0.0000060*	*0.2013*	*0.0002*	*-12*	*6*
Atlanta (2)	EL6	*0.1849*	*0.0002*	*-8*	*8*	*8*	*8*	*0.5127919*	*0.0000051*	*0.2014*	*0.0002*	*-16*	*8*
Blithfield (1)	EL6	*0.2285*	*0.0002*	*22*	*6*	*-26*	*6*	*0.5134645*	*0.0000060*	*0.2236*	*0.0002*	*-19*	*6*
Blithfield (2)	EL6	*0.1998*	*0.0002*	*-9*	*8*	*-14*	*8*	*0.5126591*	*0.0000051*	*0.1970*	*0.0002*	*-10*	*8*
St. Sauveur	EH6	0.1956	0.0002	-10	5	-9	5	0.5126239	0.0000027	0.1958	0.0001	-10	5
Abee (1)	EH4	0.1874	0.0002	-19	6	-6	6	0.5123947	0.0000060	0.1883	0.0002	-7	6
Abee (2)	EH4	0.1903	0.0002	-5	8	3	8	0.5124901	0.0000051	0.1914	0.0002	1	8
Indarch (1)	EH4	0.1953	0.0002	-14	6	-12	6	0.5126219	0.0000060	0.1958	0.0002	-13	6
Indarch (2)	EH4	0.1948	0.0002	-16	8	-14	8	0.5126109	0.0000051	0.1954	0.0002	-15	8
Av. enstatite chondrites				-10.4	4.5	-9.2	4.9				-10.4	3.4	
Queens Mercy	H6	0.1946	0.0002	-20	5	-18	5	0.5125971	0.0000027	0.1950	0.0001	-18	5
Allegan	H5	0.1952	0.0002	-16	5	-15	5	0.5126148	0.0000027	0.1955	0.0001	-15	5
Forest City	H5	0.1944	0.0002	-19	5	-16	5	0.5125989	0.0000027	0.1950	0.0001	-17	5
Pultusk	H5	0.1934	0.0002	-20	8	-16	8	0.5126079	0.0000051	0.1953	0.0002	-19	8
Ste. Marguerite (1)	H4	0.1955	0.0002	-16	6	-16	6	0.5126351	0.0000060	0.1962	0.0002	-17	6

Europe PMC Funders Author Manuscripts

Sample	Type	$^{147}Sm/^{144}ND$ measured	2se	$\mu^{142}Nd$ measured	2sd	$\mu^{142}Nd$ corrected 1	2sd	$^{143}Nd/^{144}Nd$ measured	2sd	$^{147}Sm/^{144}Nd$ calculated	2sd	$\mu^{142}Nd$ corrected 2	2sd
Ste. Marguerite (2)	H4	0.1954	0.0002	-24	8	-23	8	0.5126355	0.0000051	0.1962	0.0002	-25	8
Bruderheim	L6	0.1935	0.0002	-19	5	-16	5	0.5125629	0.0000027	0.1938	0.0001	-16	5
Farmington (2)	L5	0.1944	0.0002	-16	6	-13	6	0.5125907	0.0000060	0.1947	0.0002	-14	6
Dhurmsala	LL6	0.1965	0.0002	-14	5	-15	5	0.5126368	0.0000027	0.1963	0.0001	-15	5
Chelyabinsk	LL5	0.1963	0.0002	-18	5	-19	5	0.5126469	0.0000027	0.1966	0.0001	-19	5
Av. ordinary chondrites				-18.3	2.1	-16.7	2.0					-17.5	2.2
Allende (2)	CV3	0.1959	0.0002	-30	5	-30	5	0.5126511	0.0000027	0.1967	0.0001	-31	5
Allende (3)	CV3	0.1961	0.0002	-30	6	-31	6	0.5126644	0.0000060	0.1972	0.0002	-32	6
Allende (4)	CV3	0.1948	0.0002	-33	8	-31	8	0.5126204	0.0000051	0.1957	0.0002	-33	8
Average CV				-31.3	3.7	-30.7	1.1					-32.1	1.4
NWA5363	Ung.	0.2520	0.0005	67.1	5.9	-16.0	7.5	0.5142920	0.0000060	0.2509	0.0002	-14.2	7.4
A-ZH-5	CAI	0.2000	0.0012	-9.2	7.6	-15.2	7.8	0.5127164	0.0000051	0.1989	0.0002	-13.5	7.7

Europe PMC Funders Author Manuscripts

Extended Data Table 2

Input parameters and results of isotopic mass-balance calculations for Nd and Sm

Uncertainties for CAIs, Allende, as well as enstatite and ordinary chondrites represent two-sided Student-t 95% confidence intervals and were propagated throughout the mass balance calculation according to equation (5) in the Methods section.

	Mass balance Allende - CAIs																
	Nd (ppm)	Sm (ppm)	$^{147}Sm/^{144}Nd$	$\mu^{142}Nd$	2σ	$\mu^{145}Nd$	2σ	$\mu^{148}Nd$	2σ	$\mu^{150}Nd$	2σ	$\mu^{144}Sm$	2σ	$\mu^{148}Sm$	2σ	$\mu^{154}Sm$	2σ
CAI	14	4.54	0.1960	-12	12	-23	3	-29	7	-64	13	-234	10	59	3	-18	6
Allende	0.967	0.313	0.1960	-31	1	5	8	9	16	4	22	-80	15	-3	9	-7	13
CAI fraction = 0.03																	
Allende w/o CAI	0.564	0.183	0.1960	-45	9	27	14	39	28	56	41	39	27	-51	16	1	23
	Mass balance enstatite chondrites - CAIs																
	Nd (ppm)	Sm (ppm)	$^{147}Sm/^{144}Nd$	$\mu^{142}Nd$	2σ	$\mu^{145}Nd$	2σ	$\mu^{148}Nd$	2σ	$\mu^{150}Nd$	2σ	$\mu^{144}Sm$	2σ	$\mu^{148}Sm$	2σ	$\mu^{154}Sm$	2σ
CAI	25	8.10	0.1960	-12	12	-23	3	-29	7	-64	13	-234	10	59	3	-18	6
ECs	0.486	0.157	0.1960	-9	5	3	2	2	2	8	7	-2	8	-1	2	0	4
CAI fraction = 0.005																	
ECs w/o CAI	0.474	0.153	0.1960	-9	5	4	2	3	2	10	8	4	8	-3	2	1	4
	Mass balance ordinary chondrites - CAIs																
	Nd (ppm)	Sm (ppm)	$^{147}Sm/^{144}Nd$	$\mu^{142}Nd$	2σ	$\mu^{145}Nd$	2σ	$\mu^{148}Nd$	2σ	$\mu^{150}Nd$	2σ	$\mu^{144}Sm$	2σ	$\mu^{148}Sm$	2σ	$\mu^{154}Sm$	2σ
CAI	25	8.10	0.1960	-12	12	-23	3	-29	7	-64	13	-234	10	59	3	-18	6
OCs	0.680	0.220	0.1960	-17	2	6	3	7	3	17	5	6	7	-2	3	1	4
CAI fraction = 0.005																	
OCs w/o CAI	0.668	0.216	0.1960	-17	2	7	3	8	3	19	5	10	8	-3	3	1	5

Europe PMC Funders Author Manuscripts

Extended Data Table 3

μ^{142}Nd values corrected for nucleosynthetic anomalies.

a, Correction obtained from the intercept values of regressions through the measured meteorite Nd isotope data in μ^{142}Nd versus μ^{1XX}Nd space (*c.f.*, Fig. 3; Extended Data Fig. 4). **b**, Correction calculated from intercepts of measured data points and the slopes of *s*-process modeling27, isotopic compositions of SiC grains26, and isotopic compositions of chondrite leachates20,21 using the equation $\mu^{142}Nd_{anomaly\ corrected} = \mu^{142}Nd - \mu^{1xx}Nd \times slope$. EC: enstatite chondrites; OC: ordinary chondrites; NWA: NWA 5363; Std: processed terrestrial standards; CV w/o CAI: CAI-free Allende component as calculated from isotopic mass-balance. Regressions were calculated using ISOPLOT and uncertainties on the intercept value are 95% confidence intervals. All anomaly corrected μ^{142}Nd values calculated for the individual meteorites are indistinguishable within uncertainty, regardless of the technique used to make the corrections (*i.e.*, using regressions trough the bulk meteorite Nd data, s-process model predictions, SiC grain data or acid leachate data). The weighted averages of the anomaly corrected μ^{142}Nd values consistently range between −6±4 and −4±2 ppm relative to the mean measured JNdi-1 standard value. If all data are normalized to the mean values measured for the processed standards (**a', b'**), the anomaly corrected μ^{142}Nd values range between −4±5 and −1±2 ppm.

(a)	Nucleosynthetic anomaly corrected μ^{142}Nd in parts per million deviation relative to the mean measured JNdi-1 standard															
	regression EC, OC, NWA								regression Std, EC, OC, NWA							
correction from intercept of correction relation slope rel μ^{142}Nd	^{145}Nd	2σ	^{148}Nd	2σ	^{150}Nd	2σ	wt. av.	2σ	^{145}Nd	2σ	^{148}Nd	2σ	^{150}Nd	2σ	wt. av.	2σ
	-1.9	2.1	-0.84	9.8	-0.69	0.75			-2	1.6	-1.27	0.58	-0.73	0.3		
$\mu^{142}Nd_{anomaly\ corrected}$	-3	12	-9	74	-4	12	-4	10	-3	9	-6	4	-3	4	-4	3

(a) continued	Nucleosynthetic anomaly corrected μ^{142}Nd in parts per million deviation relative to the mean measured JNdi-1 standard															
	regression EC, OC, NWA, CV w/o CAI								regression Std, EC, OC, NWA, CV w/o CAI							
correction from intercept of correction relation slope rel μ^{142}Nd	^{145}Nd	2σ	^{148}Nd	2σ	^{150}Nd	2σ	wt. av.	2σ	^{145}Nd	2σ	^{148}Nd	2σ	^{150}Nd	2σ	wt. av.	2σ
	-1.58	0.97	-0.89	0.56	-0.72	0.54			-1.72	0.9	-1.21	0.5	-0.73	0.27		
$\mu^{142}Nd_{anomaly\ corrected}$	-5	7	-9	5	-4	9	-6	4	-4	6	-6	4	-3	4	-5	3

(b)	Nucleosynthetic anomaly corrected μ^{142}Nd in parts per million deviation relative to the mean measured JNdi-1 standard																							
	stellar model								SiC								leachates							
correction using correction relation slope rel μ^{142}Nd	^{145}Nd	2σ	^{148}Nd	2σ	^{150}Nd	2σ	wt. av.	2σ	^{145}Nd	2σ	^{148}Nd	2σ	^{150}Nd	2σ	wt. av.	2σ	^{145}Nd	2σ	^{148}Nd	2σ	^{150}Nd	2σ	wt. av.	2σ
	-1.84		-0.95		-0.61				-1.52		-0.88		-0.75				-1.61		-0.92		-0.83			
EC $\mu^{142}Nd_{anomaly\ corrected}$	-3	6	-7	5	-4	7	-5	3	-4	6	-8	5	-3	7	-5	3	-4	5	-7	9	-2	5	-4	3
OC $\mu^{142}Nd_{anomaly\ corrected}$	-6	6	-10	3	-6	3	-8	2	-8	5	-10	3	-4	4	-8	2	-7	5	-10	3	-3	4	-7	2

Europe PMC Funders Author Manuscripts

(b)	Nucleosynthetic anomaly corrected $\mu^{142}Nd$ in parts per million deviation relative to the mean measured JNdi-1 standard																									
NWA $\mu^{142}Nd_{anomaly\ corrected}$	4	13	0	10	8	16	4	7	1	12	-1	10	14	19	3	7	2	12	0	10	17	21	4	8		
wt. av. $\mu^{142}Nd_{anomaly\ corrected}$							-5	2							-5	2							-4	2		

(a')	Nucleosynthetic anomaly corrected $\mu^{142}Nd$ in parts per million deviation relative to the mean of processed standards															
	regression EC, OC, NWA								regression Std, EC, OC, NWA							
correction from intercept of correction relation slope rel $\mu^{142}Nd$	^{145}Nd	2σ	^{148}Nd	2σ	^{150}Nd	2σ	wt. av.	2σ	^{145}Nd	2σ	^{148}Nd	2σ	^{150}Nd	2σ	wt. av.	2σ
	-1.9	2.1	-0.84	9.8	-0.69	0.75			-2	1.6	-1.27	0.58	-0.73	0.3		
$\mu^{142}Nd_{anomaly\ corrected}$	-1	14	-6	100	-1	15	-1	12	-1	10	-2	5	0	5	-1	4

(a') continued	Nucleosynthetic anomaly corrected $\mu^{142}Nd$ in parts per million deviation relative to the mean of processed standards															
	regression EC, OC, NWA, CV w/o CAI								regression Std, EC, OC, NWA, CV w/o CAI							
correction from intercept of correction relation slope rel $\mu^{142}Nd$	^{145}Nd	2σ	^{148}Nd	2σ	^{150}Nd	2σ	wt. av.	2σ	^{145}Nd	2σ	^{148}Nd	2σ	^{150}Nd	2σ	wt. av.	2σ
	-1.58	0.97	-0.89	0.56	-0.72	0.54			-1.72	0.9	-1.21	0.5	-0.73	0.27		
$\mu^{142}Nd_{anomaly\ corrected}$	-3	8	-6	6	0	11	-4	5	-2	7	-2	5	0	5	-1	3

(b')	Nucleosynthetic anomaly corrected $\mu^{142}Nd$ in parts per million deviation relative to the mean of processed terrestrial standards																									
	stellar model								SiC								leachates									
correction using correction relation slope rel $\mu^{142}Nd$	^{145}Nd	2σ	^{148}Nd	2σ	^{150}Nd	2σ	wt. av.	2σ	^{145}Nd	2σ	^{148}Nd	2σ	^{150}Nd	2σ	wt. av.	2σ	^{145}Nd	2σ	^{148}Nd	2σ	^{150}Nd	2σ	wt. av.	2σ		
	-1.84		-0.95		-0.61				-1.52		-0.88		-0.75				-1.61		-0.92		-0.83					
EC $\mu^{142}Nd_{anomaly\ corrected}$	-1	6	-4	5	-1	7	-2	3	-2	6	-4	5	1	7	-2	3	-2	5	-4	9	1	5	-1	3		
OC $\mu^{142}Nd_{anomaly\ corrected}$	-4	6	-7	3	-3	3	-5	2	-6	5	-7	3	-1	4	-5	2	-6	5	-7	3	1	4	-4	2		
NWA $\mu^{142}Nd_{anomaly\ corrected}$	6	13	4	10	11	16	6	7	3	12	2	10	17	19	6	7	4	12	3	10	20	21	7	8		
wt. av. $\mu^{142}Nd_{anomaly\ corrected}$							-2	2							-2	2							-1	2		

Europe PMC Funders Author Manuscripts

Extended Data Table 4

Collateral effects of the isotopic mass-balance between Allende and CAIs for Ca, Ti, Cr, Ni, Sr, Zr, Mo, Ba.

Uncertainties represent two-sided Student-t 95% confidence intervals and were propagated throughout the mass balance calculation according to equation (5) in the Methods section. Data sources are refs. 15–18,22,28–31,37,39 and therein.

CAI fraction = 0.03	Ca (wt%)	μ^{48}Ca	2σ
CAI	10.1	370	160
Allende	1.9	392	50
Allende w/o CAI	1.6	396	67

CAI fraction = 0.03	Ti (ppm)	μ^{46}Ti	2σ	μ^{50}Ti	2σ
CAI	6042	172	12	933	69
Allende	899	67	7	365	34
Allende w/o CAI	739	40	9	221	46

CAI fraction = 0.03	Cr (ppm)	μ^{54}Cr	2σ
CAI	997	641	90
Allende	3638	87	7
Allende w/o CAI	3720	82	7

CAI fraction = 0.03	Ni (ppm)	μ^{62}Ni	2σ	μ^{64}Ni	2σ
CAI	342	117	20	247	58
Allende	14193	11	3	31	9
Allende w/o CAI	14621	11	3	31	9

CAI fraction = 0.03	Sr (ppm)	μ^{84}Sr	2σ
CAI	66	126	11
Allende	16	63	10
Allende w/o CAI	14	54	12

CAI fraction = 0.03	Zr (ppm)	μ^{91}Zr	2σ	μ^{92}Zr	2σ	μ^{96}Zr	2σ
CAI	40	0	6	-2	14	161	31
Allende	7	2	21	-3	8	110	31
Allende w/o CAI	6	2	26	-3	10	99	38

CAI fraction = 0.03	Mo (ppm)	μ^{92}Mo	2σ	μ^{94}Mo	2σ	μ^{95}Mo	2σ	μ^{97}Mo	2σ	μ^{100}Mo	2σ
CAI	3.5	274	21	123	19	197	8	89	7	131	22
Allende	1.5	287	67	210	51	168	34	94	43	100	48
Allende w/o CAI	1.4	288	72	217	55	166	37	94	47	98	52

CAI fraction = 0.03	Ba (ppm)	μ^{130}Ba	2σ	μ^{132}Ba	2σ	μ^{135}Ba	2σ	μ^{137}Ba	2σ	μ^{138}Ba	2σ
CAI	30	-40	44	-119	74	54	6	18	5	17	9
Allende	5	63	130	13	258	26	41	19	25	9	32
Allende w/o CAI	4	87	161	44	318	20	50	19	31	8	39

Supplementary Material

Refer to Web version on PubMed Central for supplementary material.

Acknowledgments

We thank the Field Museum for providing samples, Seung-Gu Lee for help setting up the chemistry in Chicago, Rick Carlson for discussions, and two referees for constructive comments. This work was funded through SNF PBE2PZ-145946 (CB); NASA (NNX14AK09G, OJ-30381-0036A, NNX15AJ25G), NSF (EAR144495, EAR150259) (ND); NASA NNH12AT84I (LB) and the ERC (Grant Agreement 616564 'ISOCORE') (TK). The work performed by LB, GB, and QS was done under the auspices of the US Department of Energy by Lawrence Livermore National Laboratory under Contract DE-AC52-07NA27344.

References

1. Bouvier A, Vervoort JD, Patchett PJ. The Lu-Hf and Sm-Nd isotopic composition of CHUR: constraints from unequilibrated chondrites and implications for the bulk composition of terrestrial planets. Earth Planet Sci Lett. 2008; 273:48–57.
2. Nakamura N. Determination of REE, Ba, Fe, Mg, Na, and K in carbonaceous and ordinary chondrites. Geochim Cosmochim Acta. 1974; 38:757–775.
3. Campbell IH, O′Neill HSC. Evidence against a chondritic Earth. Nature. 2012; 483:553–558. [PubMed: 22460899]
4. Jacobsen SB, Wasserburg GJ. Sm-Nd isotopic evolution of chondrites. Earth Planet Sci Lett. 1980; 50:139–155.
5. Meissner F, Schmidt-Ott W-D, Ziegeler L. Half-life and α-ray energy of ^{146}Sm. Z Phys A. 1987; 327:171–174.
6. Boyet M, Carlson RW. ^{142}Nd evidence for early (>4.53 Ga) global differentiation of the silicate Earth. Science. 2005; 309:576–581. [PubMed: 15961629]
7. Caro G, Bourdon B, Halliday A, Quitté G. Superchondritic Sm/Nd in Mars, Earth and the Moon. Nature. 2008; 452:336–339. [PubMed: 18354479]
8. Huang S, Jacobsen SB, Mukhopadhyay S. ^{147}Sm-^{143}Nd systematics of Earth are inconsistent with a superchondritic Sm/Nd ratio. Proceedings of the National Academy of Sciences. 2013; 110:4929–4934.
9. Jellinek AM, Jackson MG. Connections between the bulk composition, geodynamics and habitability of Earth. Nature Geosci. 2015; 8:587–593.
10. Carlson RW, Boyet M. Composition of the Earth's interior: the importance of early events. Phil Trans Roy Soc London. 2008; 366:4077–4103.
11. Bennett VC, Brandon AD, Nutman AP. Coupled ^{142}Nd-^{143}Nd isotopic evidence for Hadean mantle dynamics. Science. 2007; 318
12. Brandon AD, et al. Re-evaluating ^{142}Nd/^{144}Nd in lunar mare basalts with implications for the early evolution and bulk Sm/Nd of the Moon. Geochim Cosmochim Acta. 2009; 73:6421–6445.
13. Debaille V, Brandon AD, Yin QZ, Jacobsen B. Coupled ^{142}Nd-^{143}Nd evidence for a protracted magma ocean in Mars. Nature. 2007; 450:525–528. [PubMed: 18033291]
14. Harper CL, Jacobsen SB. Evidence from coupled ^{147}Sm-^{143}Nd and ^{146}Sm-^{142}Nd systematics for very early (4.5 Gyr) differentiation of the Earths mantle. Nature. 1992; 360:728–732.
15. Andreasen R, Sharma M. Solar nebula heterogeneity in p-process samarium and neodymium isotopes. Science. 2006; 314:806–809. [PubMed: 17023612]

16. Burkhardt C, et al. Molybdenum isotope anomalies in meteorites: Constraints on solar nebula evolution and origin of the Earth. Earth Planet Sci Lett. 2011; 312:390–400.
17. Carlson RW, Boyet M, Horan MF. Chondrite barium, neodymium, and samarium isotopic heterogeneity and early earth differentation. Science. 2007; 316:1175–1178. [PubMed: 17525335]
18. Trinquier A, et al. Origin of Nucleosynthetic Isotope Heterogeneity in the Solar Protoplanetary Disk. Science. 2009; 324:374–376. [PubMed: 19372428]
19. Sprung P, Kleine T, Scherer EE. Isotopic evidence for chondritic Lu/Hf and Sm/Nd of the Moon. Earth Planet Sci Lett. 2013; 380:77–87.
20. Boyet M, Gannoun A. Nucleosynthetic Nd isotope anomalies in primitive enstatite chondrites. Geochim Cosmochim Acta. 2013; 121:652–666.
21. Qin LP, Carlson RW, Alexander CMO. Correlated nucleosynthetic isotopic variability in Cr, Sr, Ba, Sm, Nd and Hf in Murchison and QUE 97008. Geochim Cosmochim Acta. 2011; 75:7806–7828.
22. Brennecka GA, Borg LE, Wadhwa M. Evidence for supernova injection into the solar nebula and the decoupling of r-process nucleosynthesis. Proceedings of the National Academy of Sciences. 2013; 110:17241–17246.
23. Marks NE, Borg LE, Hutcheon ID, Jacobsen B, Clayton RN. Samarium–neodymium chronology and rubidium–strontium systematics of an Allende calcium–aluminum-rich inclusion with implications for ^{146}Sm half-life. Earth Planet Sci Lett. 2014; 405:15–24.
24. Gannoun A, Boyet M, Rizo H, El Goresy A. Sm-146-Nd-142 systematics measured in enstatite chondrites reveals a heterogeneous distribution of Nd-142 in the solar nebula. Proc Natl Acad Sci U S A. 2011; 108:7693–7697. [PubMed: 21515828]
25. Rubin AE. Impact features of enstatite-rich meteorites. Chemie der Erde - Geochemistry. 2015; 75:1–28.
26. Hoppe, P., Ott, U. Mainstream silicon carbide grains from meteorites. AIP Conf Proc; 1997. p. 27-58.
27. Arlandini C, Käppeler F, Wisshak K. Neutron capture in low-mass asymptotic giant branch stars: cross sections and abundance signatures. Astrophys J. 1999; 525:886–900.
28. Akram W, Schönbächler M, Bisterzo S, Gallino R. Zirconium isotope evidence for the heterogeneous distribution of s–process materials in the solar system. Geochim Cosmochim Acta. 2015
29. Fischer-Gödde M, Burkhardt C, Kruijer TS, Kleine T. Ru isotope heterogeneity in the solar protoplanetary disk. Geochim Cosmochim Acta. 2015; 168:151–171.
30. Dauphas N, et al. Calcium-48 isotopic anomalies in bulk chondrites and achondrites: Evidence for a uniform isotopic reservoir in the inner protoplanetary disk. Earth Planet Sci Lett. 2014; 407:96–108.
31. Stracke A, et al. Refractory element fractionation in the Allende meteorite: Implications for solar nebula condensation and the chondritic composition of planetary bodies. Geochim Cosmochim Acta. 2012; 85:114–141.
32. Huss GR. Implications of isotopic anomalies and presolar grains for the formation of the formation of the solar system. Antarct Meteor Res. 2004; 17:132–152.
33. Gardner-Vandy KG, Lauretta DS, McCoy TJ. A petrologic, thermodynamic and experimental study of brachinites: Partial melt residues of an R chondrite-like precursor. Geochim Cosmochim Acta. 2013; 122:36–57.
34. Burkhardt, C., et al. NWA 5363/NWA 5400 and the Earth: Isotopic twins or just distant cousins?. 46th Lunar and Planetary Science Conference; Houston. 2015. #2732
35. Burkhardt C, Kleine T, Bourdon B, Palme H, Zipfel J, Friedrich JM, Ebel DS. Hf-W mineral isochron for Ca,Al-rich inclusions: Age of the solar system and the timing of core formation in planetesimals. Geochim Cosmochim Acta. 2008; 72:6177–6197.
36. Pourmand A, Dauphas N, Ireland TJ. A novel extraction chromatography and MC-ICP-MS technique for rapid analysis of REE, Sc and Y: Revising CI-chondrite and Post-Archean Australian Shale (PAAS) abundances. Chem Geol. 2012; 291:38–54.
37. Birck, JL. Geochemistry of non-traditional stable isotopes. Reviews in Mineralogy and Geochemistry. Johnson, CM.Beard, BL., Albarede, F., editors. Vol. 55. The Mineralogical Society of America; 2004. p. 25-64.

38. Hezel DC, Russell SS, Ross AJ, Kearsley AT. Modal abundances of CAIs: Implications for bulk chondrite element abundances and fractionations. Meteorit Planet Sci. 2008; 43:1879–1894.
39. Moynier F, et al. Planetary-scale strontium isotopic heterogeneity and the age of volatile depletion of early solar system materials. Astrophys J. 2012; 758:45.
40. Bischoff A, Keil K. Al-rich objects in ordinary chondrites: related origin of carbonaceous and ordinary chondrites and their constituents. Geochim Cosmochim Acta. 1984; 48:693–709.
41. Bischoff A, Keil K, Stöffler D. Perovskite-hibonite-spinel-bearing inclusions and Al-rich chondrules and fragments in enstatite chondrites. Chemie der Erde – Geochemistry. 1985; 44:97–106.
42. Dauphas N, Pourmand A. Thulium anomalies and rare earth element patterns in meteorites and the Earth: Nebular fractionation and the nugget effect. Geochim Cosmochim Acta. 2015; 163:234–261.
43. Nyquist LE, et al. ^{146}Sm-^{142}Nd formation interval for the lunar mantle. Geochim Cosmochim Acta. 1995; 59:2817–2837.

Europe PMC Funders Author Manuscripts

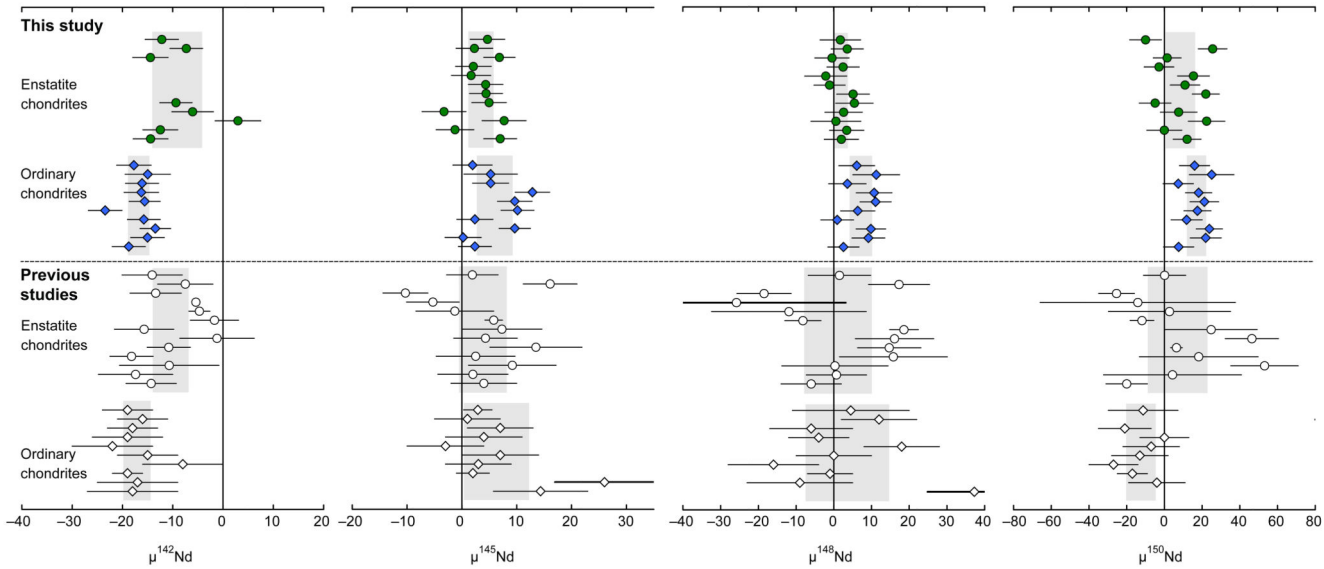

Fig. 1. Nd isotope compositions of enstatite and ordinary chondrites.

Data from this study (solid symbols) show less scatter and more precisely defined mean values (grey bars represent Student-t 95% confidence intervals of the means) than data from previous studies6,15,17,24 (open symbols), and thus reveal systematic correlated anomalies in all Nd isotopes. Uncertainties on individual data points are $2\sigma_{mean}$ of individual measurements. For definition of μ^{i}Nd see Table 1. The origin of the different μ^{150}Nd of ordinary chondrites analyzed in this study and previous studies is unclear. We note, however, that our processed standards are indistinguishable from the unprocessed JNdi-1 standard within uncertainty, rendering an analytical effect in our study unlikely. Furthermore, our μ^{150}Nd data for ordinary chondrites are correlated with anomalies in other Nd isotopes, as expected.

Europe PMC Funders Author Manuscripts

Europe PMC Funders Author Manuscripts

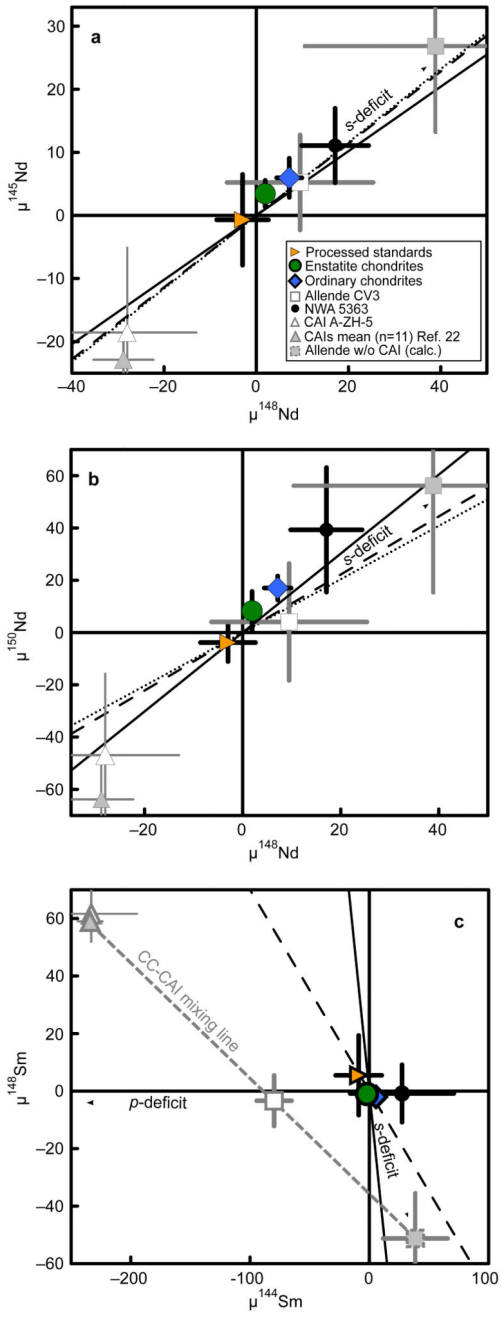

Fig. 2. Nd and Sm isotope variations among meteoritic and terrestrial samples.

(a,b) Anomalies in non-radiogenic Nd isotopes are consistent with a heterogeneous distribution of *s*-process Nd. Solid, dotted and dashed lines are mixing lines between terrestrial Nd and *s*-process Nd, calculated using modeled *s*-process compositions27, Nd data for presolar SiC grains26, and Nd data for chondrite leachates20,21. The isotopic composition measured for bulk Allende can be accounted for by admixture of CAIs to a CAI-free carbonaceous chondrite source reservoir (Allende without CAI point) characterized by a *s*-process deficit. (c) The *p*-deficit observed for bulk Allende in $\mu^{144}Sm$

can also be attributed to admixture of CAIs. Grey dashed CC-CAI line represents a mixing line calculated by subtracting CAIs from the isotopic composition measured for bulk Allende. Error bars are 95% confidence intervals.

Europe PMC Funders Author Manuscripts

Europe PMC Funders Author Manuscripts

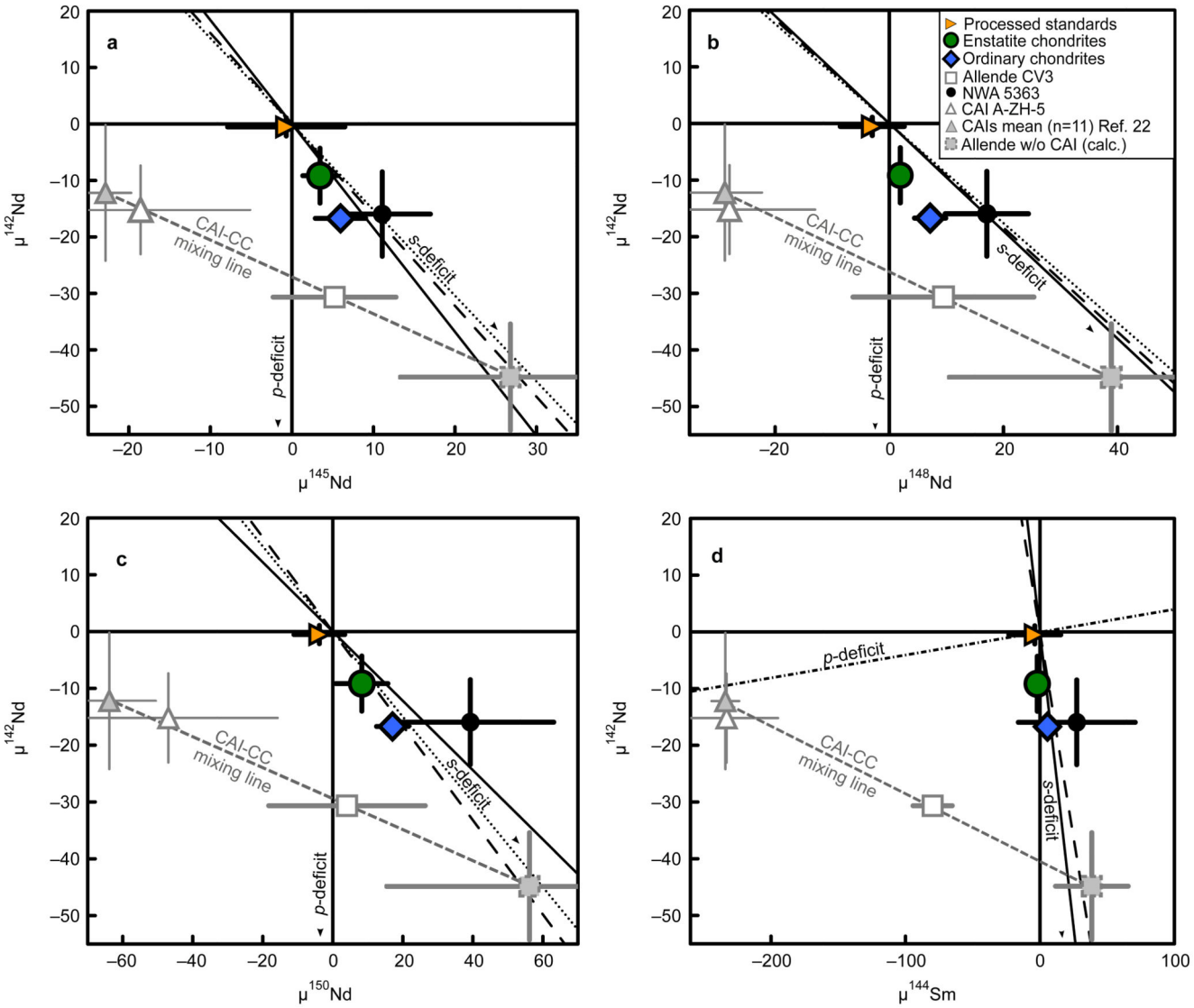

Fig. 3. Nd and Sm isotope variations among meteoritic and terrestrial samples.

(a-d) For enstatite chondrites, ordinary chondrites and NWA 5363, the μ^{142}Nd anomalies are correlated with the non-radiogenic Nd isotopes as expected for a heterogeneous distribution of *s*-process Nd. Carbonaceous chondrites plot off this correlation due to admixture of CAIs. Mass-balance indicates that a CAI-free carbonaceous chondrite source reservoir was characterized by a *s*-process deficit. Error bars are 95% confidence intervals.

Table 1

Sm/Nd ratios and Nd and Sm isotope compositions of meteoritic and terrestrial samples.

Sample	Type	$^{147}Sm/^{144}Nd$ measured	$\mu^{142}Nd$ measured	$\mu^{142}Nd$ corrected	$\mu^{145}Nd$	$\mu^{148}Nd$	$\mu^{150}Nd$	$\mu^{144}Sm$	$\mu^{148}Sm$	$\mu^{149}Sm$
Hvittis (1)	EL6	0.1999(2)	-6 (5)	-12 (5)	5 (9)	2 (5)	-10 (24)	6 (22)	1 (12)	-73 (
Hvittis (2)	EL6	0.1986(2)	-3 (6)	-7 (6)	2 (6)	4 (7)	26 (24)	-9 (43)	-1 (10)	-76 (
Hvittis (3)	EL6	0.1993(2)	-10 (8)	-14 (8)	7 (13)	0 (15)	1 (31)	0 (38)	4 (10)	-75 (
Atlanta (1)	EL6	0.1909(2)	*-5 (6)*	*3 (6)*	2 (6)	2 (7)	-3 (24)	14 (43)	0 (10)	-44 (
Atlanta (2)	EL6	0.1849(2)	*-8 (8)*	*8 (8)*	2 (13)	-2 (15)	15 (31)	-10 (43)	0 (10)	-44 (
Blithfield (1)	EL6	0.2285(2)	*22 (6)*	*-26 (6)*	4 (6)	-1 (7)	11 (24)	-2 (43)	3 (10)	-34 (
Blithfield (2)	EL6	0.1998(2)	*-9 (8)*	*-14 (8)*	4 (13)	5 (15)	22 (31)	14 (38)	0 (10)	-51 (
St. Sauveur	EH6	0.1956(2)	-10 (5)	-9 (5)	5 (9)	5 (5)	-5 (24)	-17 (22)	-6 (12)	-49 (
Abee (1)	EH4	0.1874(2)	-19 (6)	-6 (6)	-3 (6)	3 (7)	8 (24)	-18 (43)	-6 (10)	-39 (
Abee (2)	EH4	0.1903(2)	-5 (8)	3 (8)	8 (13)	1 (15)	22 (31)	-15 (43)	0 (10)	-33 (
Indarch (1)	EH4	0.1953(2)	-14 (6)	-12 (6)	-1 (6)	3 (7)	0 (24)	18 (43)	0 (10)	-35 (
Indarch (2)	EH4	0.1948(2)	-16 (8)	-14 (8)	7 (13)	2 (15)	12 (31)	-7 (43)	-5 (10)	-68 (
Av. enstatite chondrites			**-10.4 (4.5)**	**-9.2 (4.9)**	**3.4 (2.1)**	**1.9 (1.5)**	**8.3 (7.4)**	**-2 (8)**	**-1 (2)**	
Kermouve	H6	0.1926(2)						18 (22)	-1 (12)	10 (
Queens Mercy	H6	0.1946(2)	-20 (5)	-18 (5)	2 (9)	6 (5)	16 (24)	11 (22)	-2 (12)	11 (
Allegan	H5	0.1952(2)	-16 (5)	-15 (5)	5 (9)	11 (6)	25 (24)	0 (22)	-8 (12)	-12 (
Forest City	H5	0.1944(2)	-19 (5)	-16 (5)	5 (9)	4 (6)	7 (24)	-4 (22)	-12 (12)	0 (
Pultusk	H5	0.1934(2)	-20 (8)	-16 (8)	13(13)	11 (15)	18 (31)	13 (38)	2 (10)	-52 (
Ste. Marguerite (1)	H4	0.1955(2)	-16 (6)	-16 (6)	10 (6)	11 (7)	21 (24)	12 (43)	1 (10)	-16 (
Ste. Marguerite (2)	H4	0.1955(2)	-24 (8)	-23 (8)	10 (13)	6 (15)	18 (31)	0 (38)	-4 (10)	-18 (
Bruderheim	L6	0.1935(2)	-19 (5)	-16 (5)	2 (9)	1 (5)	12 (24)	-4 (22)	2 (12)	-58 (
Farmington (1)	L5	0.1944(2)						26 (22)	-4 (12)	6 (
Farmington (2)	L5	0.1944(2)	-16 (6)	-13 (6)	10 (6)	10 (7)	24 (24)	-10 (43)	-2 (10)	9 (
Dhurmsala	LL6	0.1965(2)	-14 (5)	-15 (5)	0 (9)	9 (5)	22 (24)	-12(22)	5 (12)	1 (
Paragould	LL5	0.1924(2)						22 (22)	-5 (12)	-70 (
Chelyabinsk	LL5	0.1963(2)	-18 (5)	-19 (5)	2 (9)	3 (4)	8 (24)	3 (22)	1 (12)	-8 (
Av. ordinary chondrites			**-18.3 (2.1)**	**-16.7 (2.0)**	**6.0 (3.1)**	**7.2 (2.7)**	**17.0 (4.6)**	**6 (7)**	**-2 (3)**	
Allende (1)	CV3	0.1929(2)						-85 (22)	-2 (12)	-46 (
Allende (2)	CV3	0.1959(2)	-30 (5)	-30 (5)	2 (9)	9 (4)	8 (24)	-68 (22)	-8 (12)	-31 (
Allende (3)	CV3	0.1961(2)	-30 (6)	-31 (6)	5 (6)	4 (7)	-6 (24)	-77 (22)	-8 (12)	-33 (
Allende (4)	CV3	0.1948(2)	-33 (8)	-31 (8)	8 (13)	16 (15)	11 (31)	-89 (38)	4 (10)	-29 (
Average CV			**-31.3 (3.7)**	**-30.7 (1.1)**	**5.2 (7.5)**	**9 (16)**	**4 (22)**	**-80 (15)**	**-3 (9)**	
NWA 5363	Ung.	0.2520(2)	**67.1(5.9)**	**-16.0 (7.5)**	**11 (6)**	**17.1 (7.3)**	**39 (24)**	**27 (43)**	**-1 (10)**	**-109 (**
A-ZH-5	CAI	0.2000(11)	**-9.2 (7.6)**	**-15.2 (7.8)**	**-19 (13)**	**-28 (15)**	**-47 (31)**	**-233 (38)**	**62 (10)**	**-35 (**
JNdi-1 (1)	Std		0 (5)	0 (5)	-6 (9)	-5 (5)	-2 (24)			
BHVO-2	Std	0.1484(2)	-1 (5)	-1 (5)	-2 (9)	-7 (5)	-3 (24)	-7 (22)	4 (12)	6 (
JNdi-1 (2)	Std		0 (8)	0 (8)	0 (13)	0 (15)	0 (31)			
BIR-1	Std	0.2759(3)	-2 (8)	-2 (8)	5 (13)	0 (15)	-10 (31)	-10 (38)	7 (10)	1 (
Av. processed std.			**-0.5 (1.6)**	**-0.5 (1.6)**	**-0.7 (7.2)**	**-3.0 (5.6)**	**-3.8 (7.3)**	**-9 (19)**	**5 (12)**	**4 (**

$\mu^{i}ND=[(\iota Nd/^{144}Nd)^{*}$ sample$/(\iota Nd/^{144}Nd)^{*}$standard$-1]\times 10^{6}$ and $\mu^{i}Sm=[(\iota Sm/^{152}Sm)^{*}$ sample$/(\iota Sm/^{152}Sm)^{*}$standard$-1]\times 10^{6}$ where the * superscript denotes that the ratios have been corrected for mass fractionation by internal normalizations to fixed $^{146}Nd/^{144}Nd$ and $^{147}Sm/^{152}Sm$ ratios using the exponential law. 'μ^{142}Nd corrected' denotes μ^{142}Nd corrected for radiogenic ^{142}Nd variations to a common chondritic $^{147}Sm/^{144}Nd = 0.1960$. Individual sample data represent average values of up to five measurement runs from the same filament (full data set is available in the Supplementary Materials). Repeat samples denoted (1-4) represent separate digestions processed though chemistry at different times and were run on separate filaments. Uncertainties shown in parentheses are external reproducibilities of the standard (2s.d.) or two-sided Student-t 95% confidence intervals (for group averages with n>2). The deficits in μ^{149}Sm and excesses in μ^{150}Sm present in some meteorite samples are due to thermal neutron capture reactions on ^{149}Sm during exposure to galactic cosmic rays (Extended Data Fig. 5).